Article

Chemistry & Biology

The Prototypic Cyclotide Kalata B1 Has a Unique Mechanism of Entering Cells

Graphical Abstract

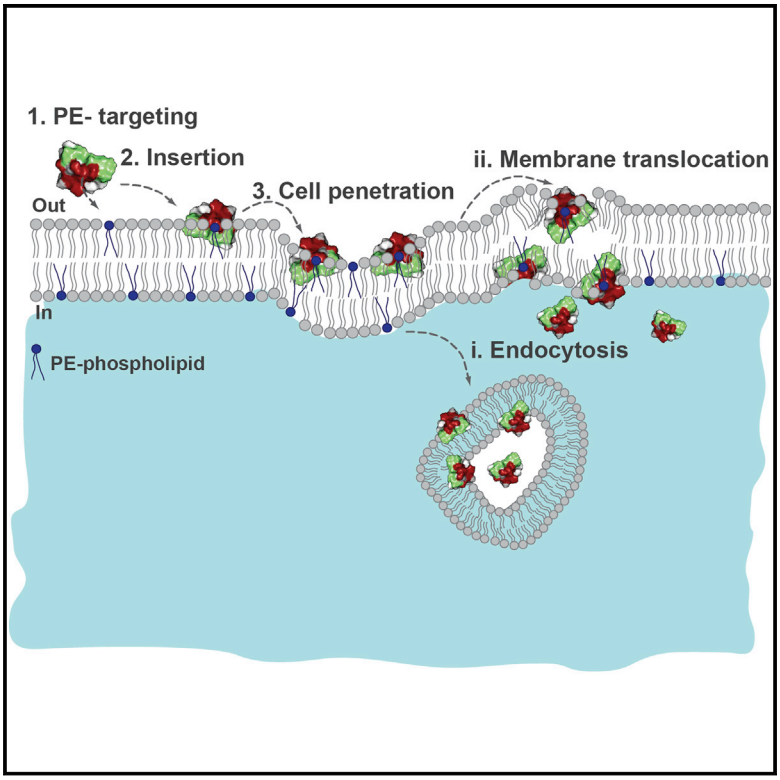

Authors

Sónia Troeira Henriques, Yen-Hua Huang, Stephanie Chaousis, ..., Aaron G. Poth, Frances Separovic, David J. Craik

Correspondence

s.henriques@uq.edu.au (S.T.H.), d.craik@imb.uq.edu.au (D.J.C.)

In Brief

Cyclotides are ultrastable cyclic peptides with potential to modulate intracellular targets. Henriques et al. show they initiate cellular internalization via the targeting of specific phospholipids followed by both endocytosis and direct membrane translocation.

Highlights

- Cyclotides are stable drug scaffolds with cell-penetrating properties
- Cyclotides enter cells via both endocytosis and direct membrane translocation
- Both pathways are initiated by targeting specific phospholipids at the cell surface
- Cyclotides are potential leads for the modulation of intracellular drug targets

Henriques et al., 2015, Chemistry & Biology *22*, 1087–1097
August 20, 2015
http://dx.doi.org/10.1016/j.chembiol.2015.07.012

CellPress

Chemistry & Biology
Article

The Prototypic Cyclotide Kalata B1 Has a Unique Mechanism of Entering Cells

Sónia Troeira Henriques,[1,*] Yen-Hua Huang,[1] Stephanie Chaousis,[1] Marc-Antoine Sani,[2] Aaron G. Poth,[1] Frances Separovic,[2] and David J. Craik[1,*]
[1]Institute for Molecular Bioscience, Chemical and Structural Biology Division, The University of Queensland, Brisbane, 4072 QLD, Australia
[2]School of Chemistry, Bio21 Molecular Science & Biotechnology Institute, University of Melbourne, 3010 VIC, Australia
*Correspondence: s.henriques@uq.edu.au (S.T.H.), d.craik@imb.uq.edu.au (D.J.C.)
http://dx.doi.org/10.1016/j.chembiol.2015.07.012

SUMMARY

Cyclotides combine the stability of disulfide-rich peptides with the intracellular accessibility of cell-penetrating peptides, giving them outstanding potential as drug scaffolds with an ability to inhibit intracellular protein-protein interactions. To realize and optimize the application of cyclotides as a drug framework and delivery system, we studied the ability of the prototypic cyclotide, kalata B1, to enter mammalian cells. We show that kalata B1 can enter cells via both endocytosis and direct membrane translocation. Both pathways are initiated by targeting phosphatidylethanolamine phospholipids at the cell surface and inducing membrane curvature. This unusual approach to initiate internalization might be harnessed to deliver drugs into cells and, in particular, cancer cells, which present a higher proportion of surface-exposed phosphatidylethanolamine phospholipids. Our findings highlight the potential of these peptides as drug leads for the modulation of traditionally "undruggable" targets, such as intracellular protein-protein interactions.

INTRODUCTION

Peptides are currently being investigated as potential leads for drug development, and have the potential to be complementary to or viable alternatives for small-molecule drugs or biologics (Craik et al., 2013; Góngora-Benítez et al., 2014). Interest in peptides as therapeutics has been driven not only by the high potency and selectivity exhibited by stable disulfide-rich peptides (e.g. conotoxin MVIIA, Prialt), but also by the discovery of cell-penetrating peptides (CPPs): short, linear, cationic peptidic sequences (e.g. TAT peptide) with the ability to breach membrane barriers and deliver proteins into cells (Henriques et al., 2006).

Cyclotides are a family of cyclic peptides isolated from plants (Burman et al., 2014; Craik et al., 1999) with a unique topology comprising a head-to-tail macrocycle and three interlocking disulfide bonds, which together lend their structures exceptional stability (Figure 1A) and resistance to proteolytic degradation (Colgrave and Craik, 2004). Cyclotides have been categorized into the Möbius, bracelet, and trypsin inhibitor subfamilies (Craik et al., 2004). Members of the Möbius and bracelet subfamilies can be found in the same plant species (e.g. *Oldenlandia affinis*) and have similar structural features and biological activities; in particular, they have hydrophobic residues exposed at the surface, and possess anti-HIV and toxic properties (Gustafson et al., 2004; Ireland et al., 2008). Despite possessing identical topology to Möbius and bracelet cyclotides, members of the trypsin inhibitor subfamily lack hydrophobic residues (Felizmenio-Quimio et al., 2001), have exquisite trypsin inhibitory activity and low cytotoxicity (Hernandez et al., 2000), and have been found exclusively in cucurbitaceous plant species (Mahatmanto et al., 2015).

The application of cyclotides as drug leads (Henriques and Craik, 2010; Jagadish and Camarero, 2010) was originally motivated by their remarkable stability, diverse biological activities, sequence variability, and amenability to chemical synthesis (Daly et al., 1999; Tam and Lu, 1998). Numerous studies have detailed the successful incorporation of linear bioactive peptides grafted onto the cyclotide framework, resulting in improved stability while maintaining potency and selectivity for their targets (Poth et al., 2013). In addition to rational design, high-throughput screening approaches that build combinatorial libraries of cyclotide analogs are being used for drug lead selection (Austin et al., 2009; Getz et al., 2011, 2013).

Recent studies in which the cell-penetrating properties of cyclotides were identified (Cascales et al., 2011; Contreras et al., 2011; Greenwood et al., 2007) revealed that in addition to being stable scaffolds, cyclotides have the potential to be used to deliver bioactive peptides into cells, and thus target intracellular proteins. This was recently confirmed in a study wherein the cyclotide *Momordica cochinchinensis* trypsin inhibitor I (MCoTI-I), engineered to incorporate a peptide epitope that mimics the N-terminal fragment of the intracellular protein p53, displayed significant resistance to degradation in vivo (Ji et al., 2013). The intracellular uptake of cyclotides belonging to the trypsin inhibitor subfamily (i.e. MCoTI-I and MCoTI-II) is reported to be dependent on endocytic routes (Cascales et al., 2011; Contreras et al., 2011; Greenwood et al., 2007) and independent of insertion into the plasma membrane (Cascales et al., 2011; D'Souza et al., 2014).

The activities reported for cyclotides belonging to the Möbius and bracelet subfamilies seem to broadly correlate with binding to cell membranes (Henriques and Craik, 2012), but little is known about their cell-penetrating properties or

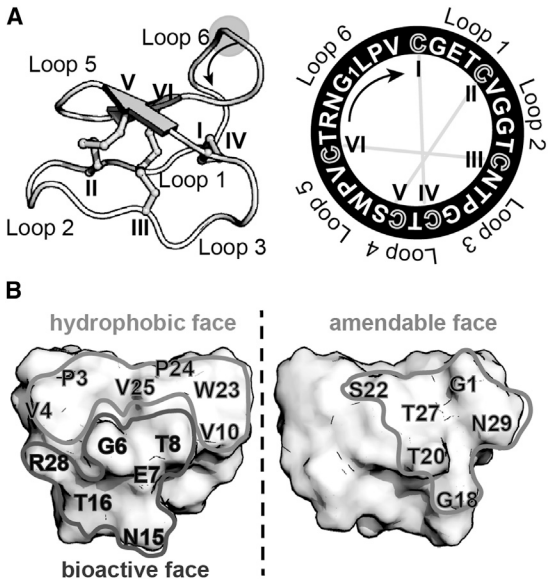

Figure 1. Structural Properties of Cyclotides

(A) Three-dimensional structure (PDB: 1NB1, left) and sequence (right) of the prototypic cyclotide, kB1. The knotted arrangement of the disulfide bonds is shown in light gray and Cys residues are labeled I to VI. The segments between Cys are named loops 1–6.

(B) Surface structure representation of kB1 in two views. Left: The hydrophobic residues (P3, V4, V10, W23, P24, and V25) of kB1 are exposed and form a patch at the surface of the molecule. Residues that are important for membrane binding localize to one side of the molecule, and include the residues in the hydrophobic patch and also those in the so-called bioactive face (G6, E7, T8, N15, T16, and R28). Right: Residues located in the "amendable" face (G1, G18, T20, S22, T27, and N29) are delineated with a line. They are named amendable because when replaced with a Lys residue they improve the membrane-binding properties of the peptide (Henriques et al., 2011; Huang et al., 2010).

See also Table S1.

the mechanism by which they gain entry into cells. These cyclotides are known to target cells through interactions with phospholipids containing phosphatidylethanolamine (PE) headgroups in the plasma membrane, followed by insertion into the lipid membrane through hydrophobic interactions (Henriques et al., 2011, 2012, 2014; Wang et al., 2012). Furthermore, when a threshold peptide concentration is reached at the cell surface the plasma membrane integrity is compromised, leading to membrane disruption followed by cell death (Henriques et al., 2012; Huang et al., 2009). Nevertheless, studies showing internalization of cyclotides without membrane permeabilization (Cascales et al., 2011) suggest that internalization occurs at concentrations below those that cause membrane disruption.

In this study we examined the cell-penetrating properties of the prototypic cyclotide, kalata B1 (kB1), and elucidated the importance of membrane-binding properties for its internalization. This study reveals that kB1 is internalized as efficiently as the gold standard CPP TAT, and shows that its uptake is dependent on its ability to target cell membranes. These mechanistic insights could assist in realizing the full potential of cyclotides as drug scaffolds that can stabilize and deliver bioactive epitopes that modulate intracellular targets.

RESULTS

Internalization of Labeled kB1 Analogs

To investigate whether the specificity of kB1 for PE phospholipids (Henriques and Craik, 2012; Henriques et al., 2011) and its ability to bind to membranes play a role in its cell-penetrating properties, four kB1 analogs including the membrane-active [T20K]kB1 and the membrane-inactive [V25K]kB1, [T16K]kB1, and [E7K]kB1 (Henriques et al., 2011) were compared on their ability to enter human cells. The analogs were labeled with a single Alexa Fluor 488 through amide bond ligation at the side chain of the single Lys residue, allowing labeling of the analogs on different faces of the kB1 surface (Figure 1B; Table S1): [T20K]kB1 on the amendable face, [V25K]kB1 on the hydrophobic face, and [T16K]kB1 and [E7K]kB1 on the bioactive face. Hereafter, all kB1 mutants are referred to by their mutation (e.g. T20K refers to [T20K]kB1), and Alexa Fluor 488-labeled peptides are indicated by an asterisk (e.g. T20K*). Notably, the labeled peptides all have the same overall charge (i.e. zero) as native kB1. The label has minimal effect on the overall hydrophobicity of the peptides, as indicated by their retention times on high-performance liquid chromatography (Table S1), and does not change the membrane-binding properties or the bioactivity of kB1 analogs (Henriques et al., 2011), as shown by surface plasmon resonance (SPR) and toxicity studies (Figures S1A and S1B); hence, T20K* can be used to examine cellular uptake of kB1 and the importance of the specificity to PE phospholipids for its internalization, whereas V25K*, T16K*, and E7K* are membrane-inactive analogs.

Internalization of kB1 mutants into HeLa cells, a cervical cancer cell line, was examined using flow cytometry (Figures 2A–2D) in non-toxic and non-permeabilizing conditions (Figure S1C). TAT was included as a positive control, and its derivative TAT-G (in which positively charged residues are replaced with Gly) (D'Souza et al., 2014), was included as a negative control to evaluate non-specific cellular internalization. As each peptide is labeled with Alexa Fluor 488 and its fluorescence emission quantum yield is insensitive to environment (Gadd et al., 2012), the mean fluorescence emission signal is directly proportional to the amount of peptide internalized into cells, whereas the percentage of fluorescent cells represents the fraction of cells that have internalized the peptide. The membrane-impermeable dye trypan blue was added to quench the fluorescence of membrane-bound peptide and/or of cells with compromised membranes (Torcato et al., 2013).

We confirmed the ability of kB1 to be internalized by cells under non-toxic and non-permeabilizing conditions (Figures 2A–2C), as cells became fluorescent upon treatment with T20K* and the percentage of fluorescent cells remains unchanged after addition of trypan blue. A drop in the mean fluorescence of T20K*-treated cells upon addition of trypan blue (Figure 2B) suggests that a portion of peptide is cell membrane-bound and is thus accessible to trypan blue (~25%, as calculated from the drop in the mean fluorescence). After 1 hr of treatment with peptide, almost all of the cells (>90%) had internalized T20K* (Figure 2A) and the amount of peptide internalized was uniformly distributed across the cell population (Figure 2C). The amount of T20K* internalized is comparable with that of TAT*

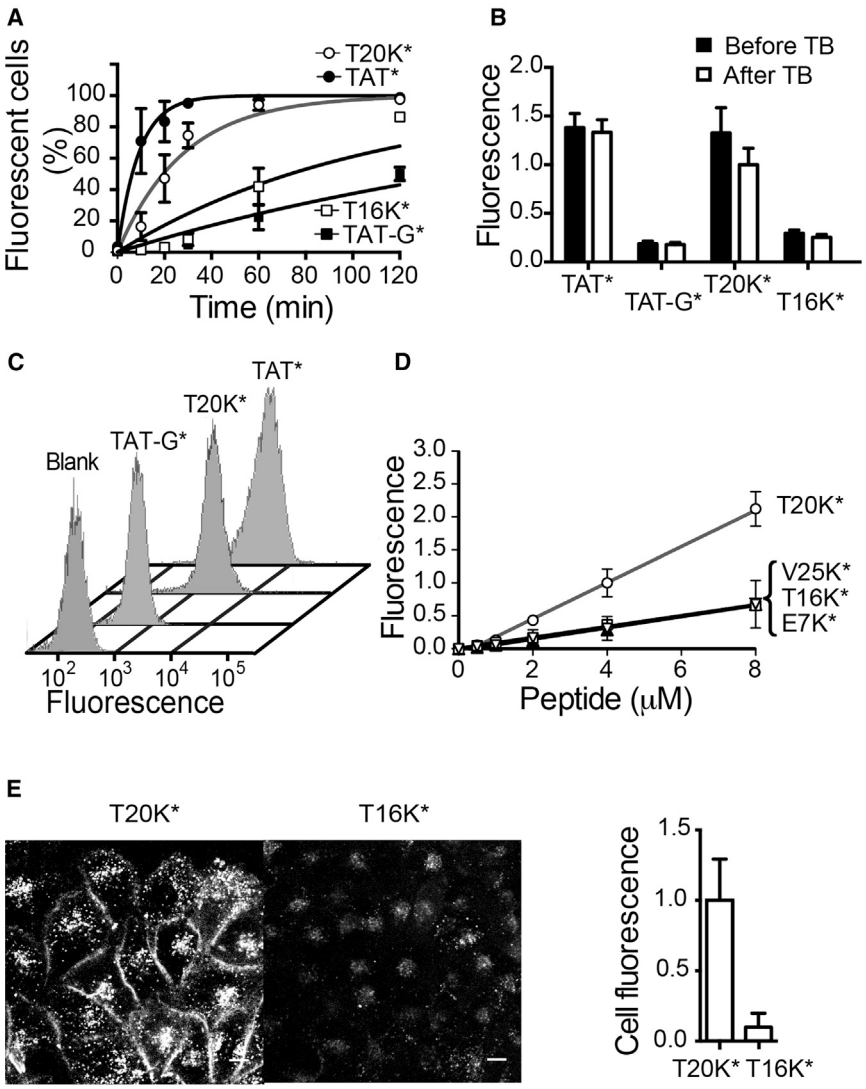

Figure 2. Internalization of kB1

(A–D) Internalization of labeled peptides into HeLa cells was followed by mean fluorescence emission intensity of Alexa Fluor 488 using flow cytometry (excitation at 488 nm and emission at 530/30 nm). Data points represent mean ± SD of three or more experiments; 10,000 cells were screened per sample.

(A) Percentage of fluorescent cells obtained upon treatment with 4 μM TAT*, TAT-G*, T20K*, or T16K* at 37°C at different incubation times and after addition of the non-permeable fluorescence quencher trypan blue (160 μg/ml, n = 3).

(B) Mean cell fluorescence signal upon treatment with 4 μM TAT*, TAT-G*, T20K*, or T16K* for 1 hr at 37°C before and after addition of trypan blue (TB). Data were normalized to the signal obtained with T20K* after trypan blue (n = 6).

(C) Fluorescence histograms of HeLa cells obtained after incubation with 4 μM TAT*, TAT-G*, or T20K* for 1 hr at 37°C and after addition of trypan blue.

(D) Mean fluorescence signal of HeLa cells obtained upon treatment with increasing concentrations of T20K*, V25K*, E7K*, or T16K* for 1 hr at 37°C and after addition of trypan blue (n = 3).

(E) Confocal live cell imaging micrographs obtained with HeLa cells after incubation with 5 μM T20K* or T16K* for 1 hr at 37°C. 1024 × 1024 pixels; scale bar, 10 μm. The bar graph shows the average cell fluorescence ± SD (n = 8 cells) in each micrograph. Values are normalized to the average of T20K*.

See also Figures S1 and S2.

(Figure 2B), whereas membrane-inactive mutants (i.e. E7K*, T16K*, and V25K*) have low internalization efficiency (Figure 2D), comparable with that of TAT-G* (Figures 2A and 2B). The same trend was observed with other cell lines tested, namely MM96L cells, a skin cancer cell line, and HFF-1, a non-cancerous skin cell line (Figures S1D and S1E). Internalization studies were conducted in either the absence or presence of inactivated fetal bovine serum (10% v/v), and no significant differences in the internalization of T20K* were detected (Figure S1F).

Internalization of T20K*, T16K*, and V25K* into HeLa cells was also examined using live cell imaging, which confirmed that T20K* is internalized to a greater extent than T16K* (Figure 2E) and V25K* (Figures S1G and S1H). The micrographs also showed that T20K* is distributed within the cell with a punctate pattern, which suggests that some peptide molecules localize in vesicle-like compartments. Examination of the fluorescence profile across the cell and comparison with the background fluorescence suggests that some peptide might be diffusely distributed within the cytoplasm (Figure S1I).

Quantification of Internalized kB1 Monitored by Mass Spectrometry

To gather information on the fraction of kB1 added extracellularly that can be internalized by HeLa cells, a quantitative methodology using multiple reaction monitoring (MRM) was employed (Figure S2A). Liquid chromatography (LC)-MRM analyses confirm that kB1 can be detected inside cells in its oxidized form (Figure S2B). After incubation of HeLa cells in media containing 8 μM kB1, non-internalized peptide was washed off, and peptide internalized and/or associated with cells was recovered after cell disruption via sonication and solubilization with acetonitrile and formic acid. The concentration of peptide detected in a re-suspension of disrupted whole cells was 5.8 ± 2.4 μM, suggesting that a large proportion of the peptide added to the growth medium can bind to the cell surface and/or be internalized. To distinguish between peptide bound to membranes and that inside cells, membrane-bound fractions were separated from soluble fractions prior to quantitation by LC-MRM (Figure S2A), where the concentrations of kB1 were found to be 1.7 ± 0.7 and 1.7 ± 1.1 μM, respectively. The similar values suggest that equal proportions of kB1 exist within the cell in membrane-bound and non-membrane-associated states. Overall, this suggests that a fraction of the peptide introduced extracellularly to HeLa cells is bound to membranes, whereas another fraction is able to cross membranes

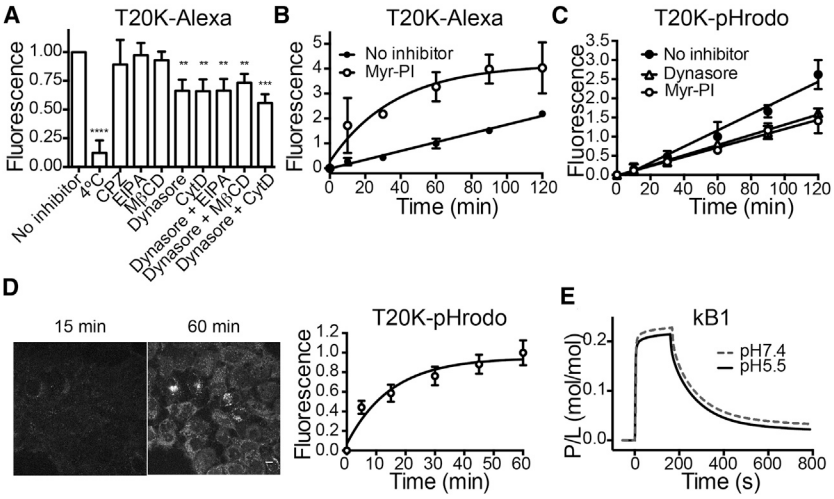

Figure 3. The Involvement of Endocytosis in the Internalization of kB1 Mutants

(A) Internalization of 4 μM T20K* into HeLa cells after 1 hr incubation at 4°C or at 37°C in the absence/presence of the endocytic inhibitors: Dynasore (80 μM), chlorpromazine (CPZ; 10 μg/ml, 28 μM), 5-(*N*-ethyl-*N*-isopropyl)-amiloride (EIPA; 10 μM), methyl-β-cyclodextrin (MβCD; 4 mM), and cytochalasin D (CytD; 20 μM), or the combination of Dynasore with EIPA, MβCD, or CytD. Internalization was followed by fluorescence emission of Alexa Fluor 488 using flow cytometry (excitation at 488 nm and emission at 530/30 nm). 10,000 cells were analyzed per sample and data points represent mean ± SD. Data were normalized to the mean fluorescence emission signal obtained with 4 μM T20K* after treatment with trypan blue (n = 6). Statistical analysis was performed by one-way ANOVA, with Bonferroni test (**p < 0.01, ***p < 0.001, ****p < 0.0001).

(B and C) Mean fluorescence emission (excitation 488 nm, emission 530/30 nm) of HeLa cells incubated at 37°C at various incubation times with (B) 4 μM T20K* without/with 30 min pre-treatment with 50 μM Myr-PI, and (C) with 4 μM T20K-pHrodo without/with 30 min pre-treatment with 80 μM Dynasore or with 50 μM Myr-PI. Data points represent mean ± SD of three experiments, and were normalized to the average at 60 min without inhibitor; 10,000 cells were analyzed per sample.

(D) Confocal live cell imaging micrographs obtained with HeLa cells upon incubation with 10 μM T20K-pHrodo at 37°C. 2048 × 2048 pixels; scale bar, 10 μm. The plot shows the average cell fluorescence integrated density (n = 9) ± SEM within the image field over time. Fluorescence integrated density was calculated using ImageJ.

(E) SPR sensorgrams obtained upon injection of 64 μM kB1 over POPC/POPE (4:1) bilayers either in buffer at pH 7.4 (10 mM HEPES buffer containing 150 mM NaCl) to mimic membrane-binding properties in the extracellular and cytoplasmic pH, or in buffer at pH 5.5 (20 mM sodium acetate buffer containing 150 mM NaCl) to examine membrane-binding affinity in the endosome compartment environment.

See also Figures S3 and S4.

and localize either in the cytoplasm or within endosome compartments.

The Role of Endocytosis for kB1 Internalization

To evaluate the potential role of endocytic pathways in the internalization of kB1 into HeLa, cellular uptake of T20K* was followed either at 4°C or after pre-treatment with a range of endocytic inhibitors at 37°C. Specifically, we used chlorpromazine (CPZ) to inhibit the clathrin-mediated pathway, 5-(N-ethyl-N-isopropyl)-amiloride (EIPA) to inhibit macropinocytosis, and methyl-β-cyclodextrin (MβCD) to inhibit lipid raft/caveolae-dependent endocytosis. In addition to the specific inhibitors, treatment with Dynasore and cytochalasin D (CytD) were also tested to assess dependence on dynamin and actin, respectively. Conditions and concentrations for each inhibitor have been previously established for HeLa cells (Chao and Raines, 2011; Duchardt et al., 2007).

Studies conducted at 4°C revealed that internalization of T20K* is inhibited at this temperature (Figure 3A) but can be restored when the temperature is increased to 37°C (Figure S3A). Decreased internalization at 4°C might result from inhibition of ATP-dependent processes, such as endocytosis, and/or from a decrease in membrane dynamics due to reduced fluidity of the lipid bilayer.

Treatment with the specific endocytic inhibitors EIPA, MβCD, and CPZ had no effect on the overall uptake of T20K*. Treatment with Dynasore or CytD, on the other hand, decreased the internalization efficiency by 34% (Figure 3A). To examine if inhibition of a specific endocytic pathway activates others, we evaluated the effect of treating the cells with Dynasore combined with EIPA, MβCD, or CytD. The combination of Dynasore with EIPA or MβCD did not result in a further decrease in internalization compared with treatment with Dynasore alone. The combination of CytD and Dynasore decreased internalization by 44% when compared with conditions without the inhibitor. These results suggest that the uptake mechanism in HeLa cells is independent of a specific endocytic pathway but partially dependent on both dynamin and actin.

To confirm whether the reduced internalization of T20K* into HeLa cells induced by Dynasore results from the role of dynamin in clathrin-dependent endocytosis, we used a dynamin inhibitory peptide (Myr-PI; myristoylated QVPSRPNARAP). This peptide is able to get into cells (Nong et al., 2003) and in doing so prevents the binding of dynamin to the adaptor protein amphiphysin, thereby preventing clathrin-dependent endocytosis by interfering with the formation of clathrin/dynamin complex and scission of vesicles (Grabs et al., 1997; Linden, 2012). Surprisingly, instead of inhibiting, treatment of cells with Myr-PI increased the internalization rate of T20K* by 3-fold at 37°C (Figure 3B) compared with non-treated cells, but had no effect on the internalization of TAT* or TAT-G* (Figure S3B). This effect in T20K*, but not in other peptides, suggests that Myr-PI modifies cell membrane properties in a way that specifically facilitates internalization of T20K* without making the membrane more permeable to other peptides, and suggests that T20K* can be internalized by a mechanism independent of endocytosis. This hypothesis is further supported by the 13-fold increase in the internalization rate of T20K* at 4°C after pre-treatment with Myr-PI at 37°C (Figure S3C) compared with non-treated cells.

As acidification of endocytic compartments is a hallmark of endocytosis, the potential involvement of an endosomal pathway was further evaluated through treatment of cells with

T20K labeled with pHrodo green, a dye that is non-fluorescent at physiological pH but exhibits an increase in fluorescence quantum yield at acidic pH (Miksa et al., 2009). Therefore, cells become fluorescent if the peptide internalizes into endocytic compartments, whereas peptide located in the cytoplasm has very weak fluorescence. Flow cytometry showed an increase in the fluorescence signal of T20K-pHrodo-treated cells with time (Figure 3C). This was also confirmed by live cell imaging with confocal microscopy (Figure 3D); initially the sample was non-fluorescent upon addition of T20K-pHrodo but cells become fluorescent over time, suggesting internalization of T20K-pHrodo into acidic compartments. Treatment of cells with Dynasore reduced the fluorescence signal (Figure 3C), which might result from a slower internalization rate and/or less peptide migrating toward more acidic compartments. These results confirm that internalization of T20K into HeLa cells is, at least partially, dependent on endocytosis and dynamin. Interestingly, treatment of cells with Myr-PI decreased the fluorescence of cells incubated with T20K-pHrodo (Figure 3C), opposite to the effect observed in the fluorescence of cells incubated with T20K* (Figure 3B). This result suggests that treatment with Myr-PI improves the overall internalization of T20K, as measured with T20K*, but reduces its internalization and progression toward the endocytic pathway, as followed with T20K-pHrodo. The progression of kB1 into endosomes is not modulated by any effect of pH on membrane-binding affinity as tested by SPR (Figure 3E); therefore, we do not anticipate a preference for acidic over neutral pH environments.

The Influence of PE Phospholipids and Membrane Fluidity on the Ability of kB1 to Translocate Membranes

Biophysical studies using model membranes were conducted to examine whether kB1 can translocate through lipid membranes. Biological membranes have asymmetric lipid distributions and commonly have a low proportion of PE exposed in the outer leaflet (e.g. ~5%) (Daleke, 2008); nevertheless, this small proportion of PE has been shown to be enough to promote binding of kB1 to both model membranes and biological cells (Henriques et al., 2011, 2014). In the current study, model membranes with or without 20% of PE phospholipids were compared to examine the potential role of PE phospholipids in the activity of kB1. This higher proportion of PE incorporated within model membranes, relative to levels in the outer leaflet of mammalian cells, was required to allow detection and quantification of the effects induced by kB1.

Giant vesicles (GVs) composed of palmitoyloleoylphosphatidylcholine (POPC) or POPC/palmitoyloleoylphosphatidylethanolamine (POPE) were incubated with kB1 and observed using confocal microscopy to evaluate effects of the peptide on membrane stability (Figure 4A). kB1 was found not to induce visible effects on POPC membranes, but induced budding and invagination in POPC/POPE membranes. As evident in GVs with multilamellae (panel 3 in Figure 4A), kB1 has the ability to translocate through the outer bilayer, and bind to and induce the same invagination in the inner lamella. The membrane-inactive mutant T16K did not induce visible effects on either POPC (data not shown) or POPC/POPE GVs (panel 4 in Figure 4A).

Previous studies suggested that in addition to specificity for PE phospholipids, membrane fluidity also affects the ability of kB1 to bind to model membranes (Henriques et al., 2012). We examined the effect of membrane fluidity upon the membrane-binding affinity of kB1 by exposing it at 25°C to lipid mixtures containing 20% of PE phospholipids within POPC or dipalmitoylphosphatidylcholine (DPPC) matrices, which respectively mimic membranes in lamellar fluid-phase and lamellar solid-phase environments. The role of the PE-phospholipid acyl chain was also examined by comparing the PE-containing phospholipids: dioleoylphosphatidylethanolamine (DOPE), POPE, dimyristoylphosphatidylethanolamine (DMPE), and dipalmitoylphosphatidylethanolamine (DPPE) (Figures 4B and 4C). kB1 has a higher affinity for PE-containing membranes with POPC than those containing the DPPC matrix, confirming a preference for membranes in the fluid phase. These results support the hypothesis that in addition to PE targeting, kB1 relies upon hydrophobic interactions to elicit efficient targeting of, and insertion into, the membrane (Henriques et al., 2011, 2012; Wang et al., 2012). We found that PE-phospholipid acyl chains also influence the affinity of kB1 for the membrane, which is inversely proportional to the transition temperature of the individual lipids as follows: DPPE < DMPE < POPE < DOPE (Figures 4B and 4C). This is the same order as the tendency of the PE phospholipids to transition from lamellar fluid phase to hexagonal phase, which can be an indication of non-lamellar events being involved in the translocation of kB1 through the lipid membrane.

The formation of hexagonal-phase and negative membrane curvature has been suggested as an intermediate step in the internalization of other CPPs (Mishra et al., 2011). Thus, to examine whether kB1 can induce hexagonal-phase formation, static ^{31}P solid-state nuclear magnetic resonance (NMR) spectroscopy was conducted using POPC/DOPE membranes. The typical spectrum profile observed with phospholipids organized in lamellar bilayers has an asymmetrical line shape and is twice the width of that observed for phospholipids organized in hexagonal phase. We found that the static ^{31}P spectrum of POPC/DOPE membranes in the absence of kB1 showed a pattern typical of lipid bilayers in a fluid lamellar phase (Figure 4D, upper panel). In the presence of kB1 (peptide-to-lipid ratio [P/L] 1:10), there was a significant reduction in the overall chemical shift anisotropy and the formation of isotropic peaks (centered at ~0 ppm), but no evidence for hexagonal-phase formation. A reduction in the chemical shift anisotropy suggests that phosphate groups are more disordered, whereas isotropic orientation indicates that kB1 induces fast tumbling of lipids, which could result from lateral diffusion of lipids in highly curved membrane domains.

To evaluate the effect of kB1 on the individual lipids, the ^{31}P isotropic chemical shifts of POPC and DOPE were resolved by high-resolution magical angle spinning (MAS) (Figure 4D, lower panel). Comparison of MAS spectra in the presence and absence of kB1 showed a downfield shift of ~0.16 ppm in the resonance of DOPE induced by kB1, whereas the resonance of POPC shifted by only 0.06 ppm (Table S2). Interestingly, the deconvoluted spectra showed that kB1 induced the formation of a third component centered at 0.20 ppm, which contributed to 15% of the overall spectrum. This is indicative of a peptide-bound population in slow exchange (Bechinger, 2005). These results confirm the ability of kB1 to bind to membranes, and suggest that kB1 has a higher affinity for DOPE lipids than POPC.

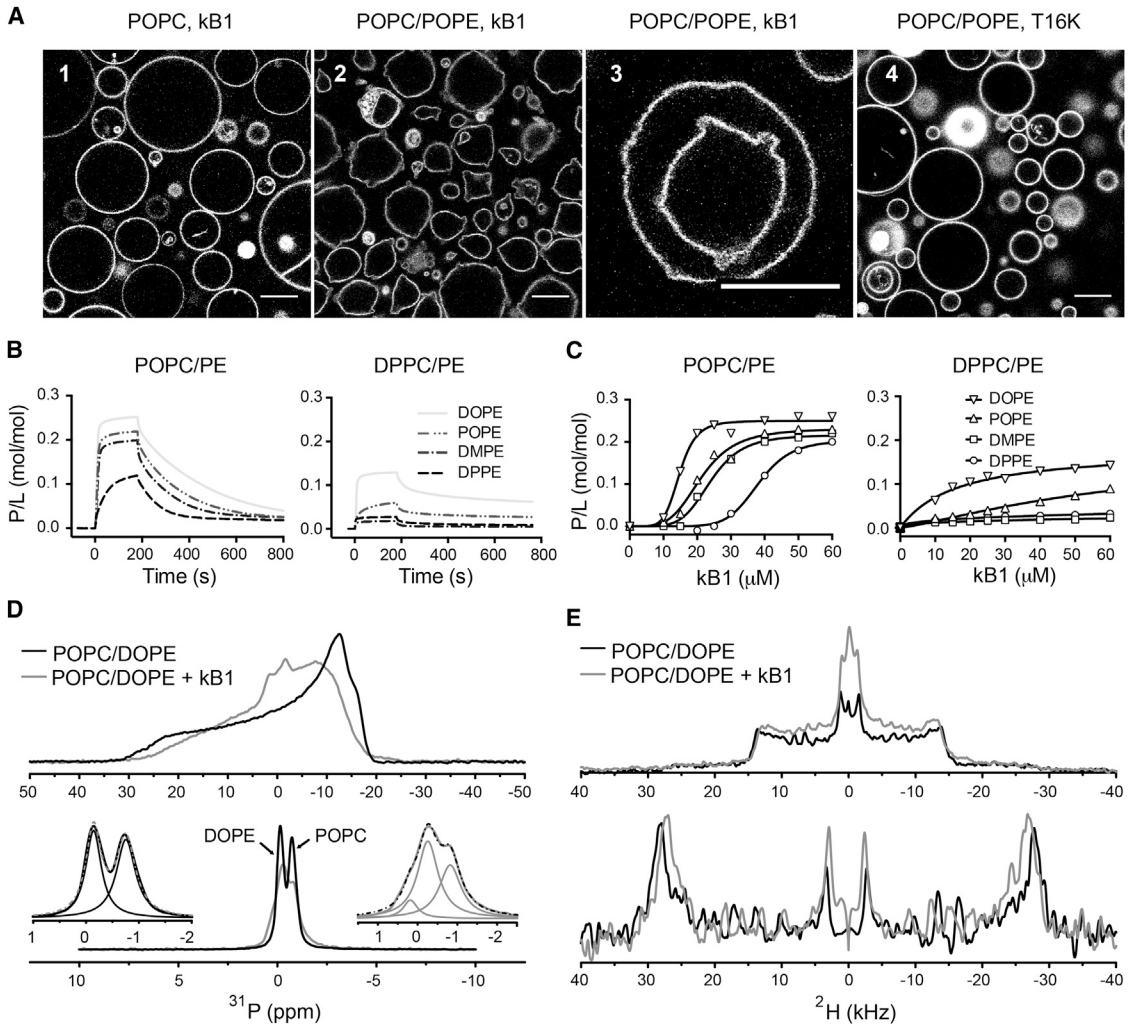

Figure 4. Effect of kB1 on Lipid Membranes and the Role of PE Phospholipids

(A) GVs labeled with 1% NBD-PE visualized by confocal microscopy after incubation with peptide (15 min): 1, POPC with 10 μM kB1 (512 × 512 pixels); 2, 3, POPC/POPE (4:1) with 5 μM kB1; 4, POPC/POPE (4:1) with 10 μM T16K (scale bar 10 μm; micrograph size is 512 × 512 pixels for 1, 2 and 4; 241 × 241 pixels for 3).

(B) SPR sensorgram obtained upon injection of 40 μM kB1 over POPC or DPPC bilayers containing 20% of DPPE, DMPE, POPE, or DOPE deposited over an L1 chip surface. kB1 was injected for 180 s and dissociation followed for 600 s. Response units were converted into peptide-to-lipid ratio (P/L; mol/mol) to normalize the response to the amount of peptide as before (Henriques et al., 2011).

(C) P/L at the end of peptide injection plotted versus peptide concentration.

(D) Static (upper) and MAS (lower) ^{31}P NMR spectra of POPC/DOPE (1:1) MLV without (black) and with (gray) kB1 at P/L 1:10. Insets show deconvolution of the MAS spectra using Lorentzian functions and their sum (dashed lines). Experiments were performed at 30°C.

(E) Pake (upper) and dePaked (lower) ^{2}H NMR spectra of POPC/d_{31}-POPC/DOPE (1:1:2) without (black) and with (gray) kB1 at P/L 1:10.

See also Table S2.

To gain more information on the perturbation of the membrane hydrophobic core, ^{2}H NMR studies were conducted with deuterated POPC (d_{31}-POPC) in POPC/DOPE mixtures (Figure 4E; Table S2). The deuterium quadrupolar splitting near the glycerol backbone (C2 to C6, see CD_2 values in Table S2) were slightly reduced while the methyl deuterons (C16, see CD_3 values) were unaffected by the presence of kB1, indicating a preference for the membrane interface region, rather than a deep insertion into the hydrophobic core of the bilayer. As observed in the ^{31}P NMR experiments, a small isotropic peak is present at 0 kHz, supporting the presence of a fast tumbling population that involves the headgroups and the acyl chains.

DISCUSSION

The goal of this study was to determine the mechanism by which kB1 enters cells. We were particularly interested in evaluating the contribution of membrane binding toward cell entry, and then distinguishing between the internalization processes of endocytosis and direct translocation through the plasma membrane. Our results suggest that kB1 can enter cells via both endocytosis and direct translocation, but binding to cell membranes appears to be the first step for both mechanisms.

We confirmed that kB1 can internalize via non-toxic and non-permeabilizing mechanisms (Figure S1C) and to an extent similar

to that of TAT (Figure 2), the gold standard CPP. Internalization of kB1 was confirmed both when conjugated to fluorescent dyes and as an unlabeled peptide. Using MRM it was possible to quantify the amount of peptide associated with cells, and to distinguish between peptide associated with membranes and peptide in solution inside cells. The significant proportions of kB1 found to have been internalized by HeLa cells (>20% of that present in media) suggests that therapeutic concentrations of designed peptide drugs based on cyclotide scaffolds can in principle be delivered to intracellular targets.

Our mechanistic studies show that the overall uptake of kB1 is potentiated by its ability to bind to cell membranes by targeting PE phospholipids (Henriques et al., 2011) and is, at least partially, dependent on endocytosis. The importance of membrane-binding properties to uptake efficiency is revealed by the markedly reduced extent of internalization for membrane-inactive compared with membrane-active kB1 analogs. T16K*, with the same mass, type of mutation, and overall structure as T20K* (Huang et al., 2010), is unable to bind membranes (Figure S1A; Henriques et al., 2011) and has a significantly lower internalization rate than T20K* in all cell lines tested (Figures 2, S1D, and S1E). As T20K* and T16K* only differ in their ability to bind PE phospholipids, the distinctive internalization efficiency is probably dependent on the ability of T20K* to target and insert into PE-containing membranes. The potential contribution of PE phospholipids in the internalization of kB1 is further supported by studies with annexin V, a protein shown to bind PE phospholipids exposed on the membrane (Marconescu and Thorpe, 2008). The presence of annexin V decreased the internalization of T20K* but did not affect the internalization of TAT* (Figure S3D).

The importance of endocytosis is supported by our work with T20K-pHrodo, which demonstrates internalization of kB1 into acidic compartments, and with endocytic inhibitors revealing that internalization into HeLa cells is partially dependent on dynamin and actin. Dynamin is a large GTPase involved in the budding and scission of nascent vesicles from the plasma membrane, and can be involved in clathrin- and caveolae-dependent endocytosis. As neither CPZ nor MβCD treatment impaired kB1 internalization, cell entry is unlikely to occur specifically by clathrin- or caveolae-dependent processes. Actin is important for cell motility and is involved in macropinocytosis, but treatment with EIPA, an inhibitor of macropinocytosis, did not decrease kB1 uptake; therefore, we excluded macropinocytosis as a specific internalization route used by kB1. The dynamin-actin complex has been suggested to have a central role in many important motile functions within the cell (Orth and McNiven, 2003). Therefore, the drop in kB1 uptake in HeLa cells treated with Dynasore and/or CytD might result from effects on the cytoskeleton and motile functions within the cell. According to this hypothesis, kB1 could enter cells by a multi-endocytic mechanism, and its internalization would be impaired by inhibition of dynamin- and actin-mediated motile functions.

Despite its ability to induce local disturbances in the lipid bilayer (Figure 4; Henriques et al., 2011), kB1 does not seem to interfere with a cell's overall endocytic activity, uptake of phospholipids, or cell membrane integrity (Figures S3E and S3F). The assembly of the endocytic machinery is restricted to the inner leaflet of the plasma membrane (Godlee and Kaksonen, 2013); therefore, we propose that kB1 is internalized by endocytosis when bound to regions with existing endocytic machinery. Such a mechanism has been demonstrated for other cargos able to internalize after diffusion into pre-formed endocytic sites (Godlee and Kaksonen, 2013). As internalization of kB1 into HeLa cells was not totally abolished upon treatment with endocytic inhibitors administered either individually or in combination, an alternative process independent of ATP might also be active.

Our studies with model membranes revealed that kB1 is able to promote vesicle budding and translocate through pure lipid bilayers containing PE phospholipids. Model membranes are characterized by symmetrical lipid composition between leaflets, but the generation of membrane curvature, as observed with kB1 in GVs, can only be explained when membrane asymmetry is generated (Graham and Kozlov, 2010). Membrane asymmetry and membrane bending can occur by direct insertion of hydrophobic domains of peptides/proteins into one of the leaflets by generating local curvature if the peptide inserts near the surface, or by expanding the total area of one monolayer, in respect to the other layer, if the peptide spans through the monolayer (Graham and Kozlov, 2010). Our SPR results suggest that kB1 inserts into the membrane rather than simply being adsorbed at the surface, and solid-state NMR showed that the insertion occurs within the headgroup region rather than the hydrophobic core. Together, these results support the notion that kB1 inserts into the outer leaflet instead of spanning the lipid bilayer, and creates the membrane asymmetry required to promote membrane bending. From a physical point of view, membrane bending requires energy, but insertion of peptides into lipid bilayers has been shown to be sufficient to meet the required energy demands of inducing such curvature (Simunovic and Bassereau, 2014). Thus, the ability of kB1 to induce bilayer bending and translocate through lipid bilayers is also probably operative in cell membranes. Previous studies suggest that kB1 is able to induce outward transbilayer movement of PE phospholipids and self-promotes its binding to the membrane by increasing the amount of PE in the outer layer (Henriques et al., 2011). A fraction as low as 0.1% of phospholipids being transferred between the two leaflets can promote vesicular structures in GVs (Farge and Devaux, 1992); therefore, upon binding to the cell membrane, kB1 might induce local effects on the plasma membrane and self-promote its internalization.

An increase in the internalization of kB1 in the presence of Myr-PI, both at 4°C and 37°C, cannot be explained by an increase in transport via endocytic pathways. Direct membrane translocation could explain why treatment with Myr-PI increased the overall internalization rate of kB1 into HeLa cells but decreased the internalization/progression through endocytic pathways. Amphiphysin is a protein that inserts into the cytosolic leaflet, and induces the membrane curvature required for the recruitment of clathrin and dynamin for vesicle formation and scission of endosomes from the cell membrane (McMahon and Boucrot, 2011). Myr-PI inhibits the binding of amphiphysin to dynamin required for the scission of clathrin-coated vesicles (Grabs et al., 1997; Linden, 2012), and as a consequence there is an accumulation of highly curved regions in the cell membrane. Our hypothesis is that regions with high inner curvature might expose more PE phospholipids, assist membrane binding, and accelerate membrane translocation of kB1, while decreasing the amount

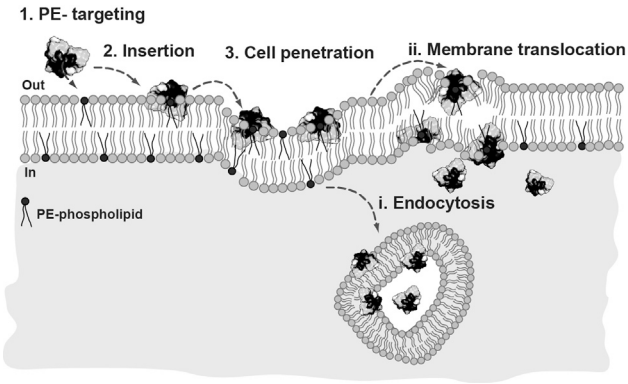

Figure 5. Model of the Mechanism of Internalization of kB1

(1) Targeting of the cell membrane through PE phospholipids increases the concentration of kB1 in the membrane vicinity; (2) insertion into the outer leaflet induces a local increase of kB1 molecules and membrane disturbances, which lead to (3) internalization through (i) endocytosis or (ii) internalization by an energy-independent process, whereby the ability to insert and induce tumbling of phospholipids and vesicle-like formation is important for the peptide to cross the lipid bilayer. The bioactive face and the hydrophobic patch are shown in dark and light gray, respectively.

of peptide available to internalize via endocytosis. This would also explain the 13-fold increase in the internalization of T20K*, but not T16K*, at 4°C upon pre-treatment with Myr-PI. Studies conducted with MM96L cells (Figures S1D and S4) further support this hypothesis and suggest that the endocytic pathway(s) by which kB1 is internalized is dependent on the cell type (e.g. treatment with CPZ induced a significant decrease in the internalization of T20K* into MM96L but not into HeLa; see Figures 3 and S4).

The internalization mechanism of kB1 proposed here is represented in Figure 5 and can be summarized as follows: the peptide targets the cell membrane through binding of the bioactive patch to PE headgroups exposed at the cell surface (step 1). This is followed by insertion into the outer membrane layer through hydrophobic interactions between the hydrophobic face of the peptide and the phospholipids (Henriques et al., 2011) (step 2). When the peptide accumulates in regions where endocytic machinery is in place, it is internalized following multi-endocytic pathways (step 3-i); actin and dynamin are probably involved in the subsequent motile functions. Alternatively, when a sufficient number of peptides is bound to the outer leaflet of the bilayer, local membrane bending occurs and the peptide internalizes by direct translocation through the plasma membrane (step 3-ii).

Based on our biophysical studies on model membranes, we hypothesize that translocation through the membrane might occur due to the formation of a non-bilayer intermediate in which the peptide molecules are in a peptide-lipid complex with PE phospholipids. Upon recovery of the lipid bilayer structure, the peptide molecules can be distributed on both sides of the bilayer, in a manner similar to that previously proposed for antimicrobial peptides (Powers et al., 2005). After this step the membrane regains integrity and re-forms a permeability barrier. The existence of a dynamic process whereby peptides and lipids are continually being redistributed between leaflets is also in agreement with previous observations that kB1 induces transbilayer movement of phospholipids in non-permeabilizing conditions, and with its ability to induce echinocyte formation in red blood cells (Henriques et al., 2011). High peptide concentrations can lead to extreme membrane deformation, leakage of cell contents, and induction of cell death (Henriques et al., 2014).

Conventional linear positively charged CPPs (e.g. TAT and R9) have a high Arg/Lys content. A single model cannot explain the internalization mechanism used by all CPPs, and indeed consensus is hard to achieve even for a single CPP. Overall, the way CPPs obtain access to the cell seems to depend on the peptide itself, experimental conditions, cargo, and cell type (Duchardt et al., 2007), but there is an increasing body of evidence suggesting that their positive charges are essential in increasing their concentration at the cell surface and in inducing cellular uptake. The fact that kB1 is internalized through targeting of PE phospholipids with subsequent insertion into the cell membrane is interesting, and indicates that cyclotides might have evolved a novel strategy to enter cells. Although other cyclotides belonging to the Möbius or bracelet subfamilies were not included in this study, we hypothesize that other native cyclotides that also are able to specifically bind PE phospholipids (Henriques et al., 2012) should be able to internalize inside cells at non-toxic and non-permeabilizing concentrations.

Cyclotides and other knotted peptides have been explored as potential drug scaffolds. It has been shown that the uptake mechanism of a given CPP affects the location and determines the bioactivity of the cargo (Duchardt et al., 2007); therefore, to enable the wider application of the cyclotide framework for delivery to intracellular targets, it is important to understand their mode of uptake. Choosing the best cyclotide framework ought to be dependent upon the cells to be targeted, the cargo, and the location of its target in the cell. For instance, MCoTI-II seems to be internalized by multiple endocytic pathways, but in particular by macropinocytosis (Cascales et al., 2011). We are unsure whether and how MCoTI-I/II peptides escape endosomes, but the fact that this peptide when grafted with a functional segment of p53 can inhibit the interaction of the oncogenic protein HdmX with p53, both located in the cytoplasm, suggests that the grafted peptide and/or an active metabolite is also active in the cytoplasm (Ji et al., 2013). kB1 seems to be able to target PE-rich membranes and to enter through endocytosis, but also to translocate through the plasma membrane in a soluble form. Therefore, kB1 presents itself as a good choice of scaffold for grafting of bioactive sequences that bind endosomal, membrane-bound, or soluble targets. Furthermore, as cancer cells typically contain a higher proportion of exposed PE phospholipids than healthy cells, kB1 might also be a useful scaffold for targeting cancer cells, and could enable inhibition of a specific cell type when equipped with a specific bioactive epitope.

SIGNIFICANCE

Intracellular protein-protein interactions have emerged as therapeutic targets but have been considered as "undruggable." Typically, protein-protein interactions involve large surface areas difficult to modulate by traditional small-molecule drugs and inaccessible to large biologics unable to internalize inside cells. Cyclotides are peptides with

exceptional stability, ability to cross cell membranes, and "plasticity" to be engineered. Accordingly, they have generated much interest as next-generation drug scaffolds with the ability to enter cells and also to be engineered to inhibit intracellular drug targets that are out of reach of conventional drugs. Prior to the development and broad application of these potential drug scaffolds, it is important to understand their mode of action. Here we characterize how kalata B1, the prototypic cyclotide, crosses the cell membrane barrier. This information can be applied in tailoring engineered cyclotides for specific intracellular targets, and in the development of drug-discovery programs for the development of stable delivery systems.

EXPERIMENTAL PROCEDURES

Additional details on the experimental procedures are provided in the Supplemental Information.

Peptide Extraction and Synthesis

Native kB1 was isolated from *Oldenlandia affinis* (Plan et al., 2007), and Lys mutants of kB1 were synthesized and purified as described previously (Huang et al., 2010). The linear peptides were synthesized using an automated peptide synthesizer (Symphony peptide synthesizer, Protein Technologies) as described previously (D'Souza et al., 2014).

Peptide Labeling

Single Lys peptides were labeled with Alexa Fluor 488 sulfodichlorophenol ester or pHrodo green sulfotetrafluorophenyl ester (Life Technologies) through amide-bound ligation (Torcato et al., 2013).

Internalization of kB1 into Cells Followed by Flow Cytometry

Internalization of labeled peptides was evaluated using a BD FACSCanto II flow cytometer, as described previously (D'Souza et al., 2014; Torcato et al., 2013).

Internalization Followed by Confocal Microscopy

HeLa cells were incubated with T20K*, V25K*, T16K*, or T20K-pHrodo and imaged at 37°C using an inverted LSM 710 confocal laser scanning microscope (Zeiss) equipped with a cage with temperature control.

Internalization Followed by Mass Spectrometry

HeLa cells were incubated with kB1 for 1 hr at 37°C. To distinguish between membrane-bound and soluble peptide, cells were disrupted and cell debris separated from supernatant. To estimate the amount of peptide associated with the "whole cell," cell debris was not separated from supernatant. A standard curve was prepared by solubilizing peptide stocks in PBS. A linear acetonitrile gradient was used to separate sample components on a Phenomenex Kinetex C18 column (100 × 2.1 mm, 1.7 μm particle size, 100 Å pore size) at a flow rate of 0.4 ml min^{-1}, and analyte MRMs monitored using a 4000 QTRAP tandem mass spectrometry system (AB/Sciex, Foster City, USA). The peptide concentration in each sample was calculated based on the standard curve.

Preparation of Liposomes by Extrusion

Synthetic lipids (POPC, DPPC, DMPC, DMPE, DOPC, DOPE, 1-palmitoyl-2(6-nitrobenzoxadiazole-aminocaproyl)-glycerophosphocholine, and 1-palmitoyl-2(6-nitrobenzoxadiazole-aminocaproyl)-glycerophosphoethanolamine [NBD-PE]) were obtained from Avanti Polar Lipids. Unless otherwise stated, vesicle suspensions were prepared in 10 mM HEPES buffer (pH 7.4) containing 150 mM NaCl, and small unilamellar vesicles (50 nm diameter) were prepared by freeze-thaw fracturing and sized by extrusion following protocols previously optimized (Henriques et al., 2008).

Peptide-Membrane Interactions Followed by SPR

Unless otherwise stated, SPR experiments were conducted at 25°C with an L1 biosensor chip in a Biacore 3000 instrument (GE Healthcare) and using 10 mM HEPES buffer (pH 7.4) containing 150 mM NaCl as running buffer. Peptides were injected over bilayers deposited onto the chip at 25°C and response units normalized to P/L as previously detailed (Henriques et al., 2011, 2012).

Preparation of GVs and Imaging by Confocal Microscopy

GVs labeled with 1% NBD-PE were prepared in 200 mM sucrose solution by electroformation using indium tin oxide-coated glass slides (surface resistivity 30–60 Ω, Sigma). GV suspensions were excited at 488 nm and images recorded upon addition of kB1 or T16K (5 or 10 μM) using an inverted LSM 510 confocal laser scanning microscope (Zeiss).

Solid-State NMR Experiments

Multilamellar vesicles in the presence or absence of kB1 (peptide/lipid molar ratio 10:1) were resuspended with Tris buffer (30 mM Tris [pH 7.4], 100 mM NaCl) to 75% hydration and packed into a 5-mm rotor. ^{2}H NMR experiments were performed on a Varian Inova 300-MHz spectrometer using a 5-mm Auto-MAS double resonance probe (Varian), and spectra were collected as described previously (Weber et al., 2012). Proton-decoupled ^{31}P NMR spectra were collected at 242.5 MHz resonance frequency using a 4.5-μs π/2 pulse, 3 s recycle delay, 125 kHz spectral width, and a SPINAL decoupling scheme. MAS ^{31}P experiments were performed at 10-kHz spinning speed with an acquisition time of 20 ms using a SPINAL-64 decoupling scheme of 48 kHz strength and a minimum of 512 scans.

SUPPLEMENTAL INFORMATION

Supplemental Information includes Supplemental Experimental Procedures, four figures, and two tables and can be found with this article online at http://dx.doi.org/10.1016/j.chembiol.2015.07.012.

ACKNOWLEDGMENTS

S.T.H. is supported by a Discovery Early Career Research Award (grant ID DE120103152) from the Australian Research Council. D.J.C. is a National Health and Medical Research Council Professorial Fellow (grant ID APP1026501). Dr. Oleksiy Kovtun (IMB, UQ) is acknowledged for the help in the preparation of the GVs. Confocal microscopy imaging was performed at the Australian Cancer Research Foundation (ACRF)/IMB Dynamic Imaging Facility for Cancer Biology established with support of ACRF. We thank John Griffin (IMB, UQ) for technical assistance with confocal microscopy imaging. We thank Olivier Cheneval (IMB, UQ) and Phillip Walsh (IMB, UQ) for assistance in peptide synthesis and purification, and Dr. Nicole Lawrence (IMB, UQ) for assistance with cell culture and bioassays. NHMRC is acknowledged for funding this project (grant ID APP1084965).

Received: February 24, 2015
Revised: June 20, 2015
Accepted: July 8, 2015
Published: August 13, 2015

REFERENCES

Austin, J., Wang, W., Puttamadappa, S., Shekhtman, A., and Camarero, J.A. (2009). Biosynthesis and biological screening of a genetically encoded library based on the cyclotide MCoTI-I. Chembiochem *10*, 2663–2670.

Bechinger, B. (2005). Detergent-like properties of magainin antibiotic peptides: a ^{31}P solid-state NMR spectroscopy study. Biochim. Biophys. Acta *1712*, 101–108.

Burman, R., Gunasekera, S., Strömstedt, A.A., and Göransson, U. (2014). Chemistry and biology of cyclotides: circular plant peptides outside the box. J. Nat. Prod. *77*, 724–736.

Cascales, L., Henriques, S.T., Kerr, M.C., Huang, Y.-H., Sweet, M.J., Daly, N.L., and Craik, D.J. (2011). Identification and characterization of a new family of cell-penetrating peptides: cyclic cell-penetrating peptides. J. Biol. Chem. *286*, 36932–36943.

Chao, T.-Y., and Raines, R.T. (2011). Mechanism of ribonuclease A endocytosis: analogies to cell-penetrating peptides. Biochemistry *50*, 8374–8382.

Colgrave, M.L., and Craik, D.J. (2004). Thermal, chemical, and enzymatic stability of the cyclotide kalata B1: the importance of the cyclic cystine knot. Biochemistry *43*, 5965–5975.

Contreras, J., Elnagar, A.Y.O., Hamm-Alvarez, S.F., and Camarero, J.A. (2011). Cellular uptake of cyclotide MCoTI-I follows multiple endocytic pathways. J. Control Release *155*, 134–143.

Craik, D.J., Daly, N.L., Bond, T., and Waine, C. (1999). Plant cyclotides: a unique family of cyclic and knotted proteins that defines the cyclic cystine knot structural motif. J. Mol. Biol. *294*, 1327–1336.

Craik, D.J., Daly, N.L., Mulvenna, J., Plan, M.R., and Trabi, M. (2004). Discovery, structure and biological activities of the cyclotides. Curr. Protein Pept. Sci. *5*, 297–315.

Craik, D.J., Fairlie, D.P., Liras, S., and Price, D. (2013). The future of peptide-based drugs. Chem. Biol. Drug Des. *81*, 136–147.

D'Souza, C., Henriques, S.T., Wang, C.K., and Craik, D.J. (2014). Structural parameters modulating the cellular uptake of disulfide-rich cyclic cell-penetrating peptides: MCoTI-II and SFTI-1. Eur. J. Med. Chem. *88*, 10–18.

Daleke, D.L. (2008). Regulation of phospholipid asymmetry in the erythrocyte membrane. Curr. Opin. Hematol. *15*, 191–195.

Daly, N.L., Love, S., Alewood, P.F., and Craik, D.J. (1999). Chemical synthesis and folding pathways of large cyclic polypeptides: studies of the cystine knot polypeptide kalata B1. Biochemistry *38*, 10606–10614.

Duchardt, F., Fotin-Mleczek, M., Schwarz, H., Fischer, R., and Brock, R. (2007). A comprehensive model for the cellular uptake of cationic cell-penetrating peptides. Traffic *8*, 848–866.

Farge, E., and Devaux, P.F. (1992). Shape changes of giant liposomes induced by an asymmetric transmembrane distribution of phospholipids. Biophys. J. *61*, 347–357.

Felizmenio-Quimio, M.E., Daly, N.L., and Craik, D.J. (2001). Circular proteins in plants: solution structure of a novel macrocyclic trypsin inhibitor from *Momordica cochinchinensis*. J. Biol. Chem. *276*, 22875–22882.

Gadd, J.C., Fujimoto, B.S., Bajjalieh, S.M., and Chiu, D.T. (2012). Single-molecule fluorescence quantification with a photobleached internal standard. Anal. Chem. *84*, 10522–10525.

Getz, J.A., Rice, J.J., and Daugherty, P.S. (2011). Protease-resistant peptide ligands from a knottin scaffold library. ACS Chem. Biol. *6*, 837–844.

Getz, J.A., Cheneval, O., Craik, D.J., and Daugherty, P.S. (2013). Design of a cyclotide antagonist of neuropilin-1 and -2 that potently inhibits endothelial cell migration. ACS Chem. Biol. *8*, 1147–1154.

Godlee, C., and Kaksonen, M. (2013). Review series: from uncertain beginnings: initiation mechanisms of clathrin-mediated endocytosis. J. Cell Biol. *203*, 717–725.

Góngora-Benítez, M., Tulla-Puche, J., and Albericio, F. (2014). Multifaceted roles of disulfide bonds. Peptides as therapeutics. Chem. Rev. *114*, 901–926.

Grabs, D., Slepnev, V.I., Songyang, Z., David, C., Lynch, M., Cantley, L.C., and De Camilli, P. (1997). The SH3 domain of amphiphysin binds the proline-rich domain of dynamin at a single site that defines a new SH3 binding consensus sequence. J. Biol. Chem. *272*, 13419–13425.

Graham, T.R., and Kozlov, M.M. (2010). Interplay of proteins and lipids in generating membrane curvature. Curr. Opin. Cell Biol. *22*, 430–436.

Greenwood, K.P., Daly, N.L., Brown, D.L., Stow, J.L., and Craik, D.J. (2007). The cyclic cystine knot miniprotein MCoTI-II is internalized into cells by macropinocytosis. Int. J. Biochem. Cell Biol. *39*, 2252–2264.

Gustafson, K.R., McKee, T.C., and Bokesch, H.R. (2004). Anti-HIV cyclotides. Curr. Protein Pept. Sci. *5*, 331–340.

Henriques, S.T., and Craik, D.J. (2010). Cyclotides as templates in drug design. Drug Discov. Today *15*, 57–64.

Henriques, S.T., and Craik, D.J. (2012). Importance of the cell membrane on the mechanism of action of cyclotides. ACS Chem. Biol. *7*, 626–636.

Henriques, S.T., Melo, M.N., and Castanho, M.A.R.B. (2006). Cell-penetrating peptides and antimicrobial peptides: how different are they? Biochem. J. *399*, 1–7.

Henriques, S.T., Pattenden, L.K., Aguilar, M.-I., and Castanho, M.A.R.B. (2008). PrP(106-126) does not interact with membranes under physiological conditions. Biophys. J. *95*, 1877–1889.

Henriques, S.T., Huang, Y.-H., Rosengren, K.J., Franquelim, H.G., Carvalho, F.A., Johnson, A., Sonza, S., Tachedjian, G., Castanho, M.A.R.B., Daly, N.L., et al. (2011). Decoding the membrane activity of the cyclotide kalata B1: the importance of phosphatidylethanolamine phospholipids and lipid organization on hemolytic and anti-HIV activities. J. Biol. Chem. *286*, 24231–24241.

Henriques, S.T., Huang, Y.-H., Castanho, M.A.R.B., Bagatolli, L.A., Sonza, S., Tachedjian, G., Daly, N.L., and Craik, D.J. (2012). Phosphatidylethanolamine binding is a conserved feature of cyclotide-membrane interactions. J. Biol. Chem. *287*, 33629–33643.

Henriques, S.T., Huang, Y.-H., Chaousis, S., Wang, C.K., and Craik, D.J. (2014). Anticancer and toxic properties of cyclotides are dependent on phosphatidylethanolamine phospholipid targeting. Chembiochem *15*, 1956–1965.

Hernandez, J.F., Gagnon, J., Chiche, L., Nguyen, T.M., Andrieu, J.P., Heitz, A., Trinh Hong, T., Pham, T.T., and Le-Nguyen, D. (2000). Squash trypsin inhibitors from *Momordica cochinchinensis* exhibit an atypical macrocyclic structure. Biochemistry *39*, 5722–5730.

Huang, Y.-H., Colgrave, M.L., Daly, N.L., Keleshian, A., Martinac, B., and Craik, D.J. (2009). The biological activity of the prototypic cyclotide kalata b1 is modulated by the formation of multimeric pores. J. Biol. Chem. *284*, 20699–20707.

Huang, Y.-H., Colgrave, M.L., Clark, R.J., Kotze, A.C., and Craik, D.J. (2010). Lysine-scanning mutagenesis reveals an amendable face of the cyclotide kalata B1 for the optimization of nematocidal activity. J. Biol. Chem. *285*, 10797–10805.

Ireland, D.C., Wang, C.K.L., Wilson, J.A., Gustafson, K.R., and Craik, D.J. (2008). Cyclotides as natural anti-HIV agents. Biopolymers *90*, 51–60.

Jagadish, K., and Camarero, J.A. (2010). Cyclotides, a promising molecular scaffold for peptide-based therapeutics. Biopolymers *94*, 611–616.

Ji, Y., Majumder, S., Millard, M., Borra, R., Bi, T., Elnagar, A.Y., Neamati, N., Shekhtman, A., and Camarero, J.A. (2013). In vivo activation of the p53 tumor suppressor pathway by an engineered cyclotide. J. Am. Chem. Soc. *135*, 11623–11633.

Linden, D.J. (2012). A late phase of LTD in cultured cerebellar Purkinje cells requires persistent dynamin-mediated endocytosis. J. Neurophysiol. *107*, 448–454.

Mahatmanto, T., Mylne, J.S., Poth, A.G., Swedberg, J.E., Kaas, Q., Schaefer, H., and Craik, D.J. (2015). The evolution of momordica cyclic peptides. Mol. Biol. Evol. *32*, 392–405.

Marconescu, A., and Thorpe, P.E. (2008). Coincident exposure of phosphatidylethanolamine and anionic phospholipids on the surface of irradiated cells. Biochim. Biophys. Acta *1778*, 2217–2224.

McMahon, H.T., and Boucrot, E. (2011). Molecular mechanism and physiological functions of clathrin-mediated endocytosis. Nat. Rev. Mol. Cell Biol. *12*, 517–533.

Miksa, M., Komura, H., Wu, R., Shah, K.G., and Wang, P. (2009). A novel method to determine the engulfment of apoptotic cells by macrophages using pHrodo succinimidyl ester. J. Immunol. Methods *342*, 71–77.

Mishra, A., Lai, G.H., Schmidt, N.W., Sun, V.Z., Rodriguez, A.R., Tong, R., Tang, L., Cheng, J., Deming, T.J., Kamei, D.T., et al. (2011). Translocation of HIV TAT peptide and analogues induced by multiplexed membrane and cytoskeletal interactions. Proc. Natl. Acad. Sci. USA *108*, 16883–16888.

Nong, Y., Huang, Y.-Q., Ju, W., Kalia, L.V., Ahmadian, G., Wang, Y.T., and Salter, M.W. (2003). Glycine binding primes NMDA receptor internalization. Nature *422*, 302–307.

Orth, J.D., and McNiven, M.A. (2003). Dynamin at the actin-membrane interface. Curr. Opin. Cell Biol. *15*, 31–39.

Plan, M.R.R., Göransson, U., Clark, R.J., Daly, N.L., Colgrave, M.L., and Craik, D.J. (2007). The cyclotide fingerprint in *Oldenlandia affinis*: elucidation of chemically modified, linear and novel macrocyclic peptides. Chembiochem *8*, 1001–1011.

Poth, A.G., Chan, L.Y., and Craik, D.J. (2013). Cyclotides as grafting frameworks for protein engineering and drug design applications. Biopolymers *100*, 480–491.

Powers, J.-P.S., Tan, A., Ramamoorthy, A., and Hancock, R.E.W. (2005). Solution structure and interaction of the antimicrobial polyphemusins with lipid membranes. Biochemistry *44*, 15504–15513.

Simunovic, M., and Bassereau, P. (2014). Reshaping biological membranes in endocytosis: crossing the configurational space of membrane-protein interactions. Biol. Chem. *395*, 275–283.

Tam, J.P., and Lu, Y.A. (1998). A biomimetic strategy in the synthesis and fragmentation of cyclic protein. Protein Sci. *7*, 1583–1592.

Torcato, I.M., Huang, Y.-H., Franquelim, H.G., Gaspar, D.D., Craik, D.J., Castanho, M.A.R.B., and Henriques, S.T. (2013). The antimicrobial activity of Sub3 is dependent on membrane binding and cell-penetrating ability. Chembiochem *14*, 2013–2022.

Wang, C.K., Wacklin, H.P., and Craik, D.J. (2012). Cyclotides insert into lipid bilayers to form membrane pores and destabilize the membrane through hydrophobic and phosphoethanolamine-specific interactions. J. Biol. Chem. *287*, 43884–43898.

Weber, D.K., Gehman, J.D., Separovic, F., and Sani, M.-A. (2012). Copper modulation of amyloid beta 42 interactions with model membranes. Aust. J. Chem. *65*, 472–479.